University of Baghdad
College of Engineering
JE
JOURNAL OF ENGINEERING

Journal of Engineering
journal homepage: www.joe.uobaghdad.edu.iq
Number 5 Volume 26 May 2020

Mechanical and Energy Engineering

Thermal Efficiency for Passive Solar Chimney with and Without Heat Storage material

Dr.Talib K. Murtadha
Assistant Professor
Mechanical Eng. Dep.
Engineering College
Mutah University/ Jordan
talib_km@yahoo.com

Dr.Hussien M. Salih
Assistant Professor
Electro-Mech. Eng. Dep
University of Technology
Baghdad/Iraq
hussein_maj@yahoo.com

Dr.Ali D.Salman *
Lecturer
Mechanical Eng. Dep.
University of Technology
Baghdad/Iraq
aligaphory@yahoo.com

ABSTRACT

In this study, a different design of passive air Solar Chimney(SC)was tested by installing it in the south wall of insulated test room in Baghdad city. The SC was designed from vertical and inclined parts connected serially together, the vertical SC (first part) has a single pass and Thermal Energy Storage Box Collector (TESB (refined paraffin wax as Phase Change Material(PCM)-Copper Foam Matrix(CFM))), while the inclined SC was designed in single pass, double passes and double pass with TESB (semi refined paraffin wax with copper foam matrix) with selective working angle ((30^o, 45^o and 60^o). A computational model was employed and solved by Finite Volume Method (FVM) to simulate the air induced through the test room by SC effect. The governing equation of Computational Fluid Dynamic (CFD) model was developed by the effective heat capacity method equation to describe the heat storage and release from PCM-CFM. Practical and computational Results referred to increase in thermal conductivity of the paraffin wax that supported by CFM than 10 times, while the ventilation effect is still active for hours after sun set amount. The maximum ventilation mass flow rate with TESB collector was 36.651 kg/hr., when the overall discharge coefficient equals 0.371. Also, the experimental results referred to the best working angle range 45~60^o, while the highest approaching temperature (between air and collector) was appeared for the double passes flat plate collector. Results gave higher heat storage efficiency 47% when the maximum solar radiation 780 W/m^2 at 12.00 pm, and the energy summation through duration of charging time was 18460 kJ. Double passes SC at 60^o angle presented the highest efficiency with value approaching to 73%, while TESB collector efficiency depicted highest efficiency value 70% at 12:00 pm.

Keywords: Solar Chimney, Efficiency, Paraffin wax, Copper foam matrix, phase change material

*Corresponding author
Peer review under the responsibility of University of Baghdad.
https://doi.org/10.31026/j.eng.2020.05.01

Article received: 12 /3/2019
Article accepted:22/6/2019
Article published:1/5/2020

الكفاءة الحرارية للمدخنةِ الشمسيةِ السلبيةِ مَع وبدون مادّةِ الخزنِ الحراريةِ

د. طالب كشاش مرتضى
أستاذ متمرس
قسم الهندسة الميكانيكية
جامعة مؤتة، الأردن

د. حسين مجيد صالح
أستاذ مساعد
قسم الهندسة الكهروميكانيكية
الجامعة التكنلوجية، بغداد، العراق

د. علي داود سلمان *
مدرس
قسم الهندسة الميكانيكية
الجامعة التكنلوجية، بغداد، العراق

الخلاصة

في هذه الدراسة تم اختبار تصاميم مختلفة من مدخنة الهواء الشمسية السلبية من خلال نصبها عند الجدار الجنوبي لغرفة اختبار معزولة مصممه لهذا الغرض. المدخنة الشمسية تتألف من جزء عمودي ذي ممر هواء احادي مع خزان حراري شمسي يحوي مادة الخزن المتمثلة بشمع برافيني نقي مدعم برغوة النحاس، اما جزء المدخنة المائل والذي تم اختباره بممر احادي، ممر ثنائي وممر ثنائي مع خزان حرارة شمسي يحوي مادة الخزن المتمثلة بشمع برافيني شبه نقي مدعم برغوة النحاس. تم الاختبار للمدخنة المائلة ضمن زوايا ميل منتقاة ($30^o, 45^o, 60^o$). تم بناء نموذج حسابي وحله باستخدام طريقة الحجوم المحددة لمحاكاة جريان الهواء خلال حيز الاختبار بتأثير المدخنة الشمسية ودعمت معادلاته الحاكمة من خلال توظيف طريقة السعة الحرارية المؤثرة لوصف الحرارة المخزونة والمتحررة للمنطقة ثنائية الطور من الشمع بالإضافة الى المناطق احادية الطور من الصلب والسائل للشمع المدعم برغوة النحاس. اظهرت النتائج العملية، ونتائج النموذج الحسابي الى زيادة الموصلية الحرارية للشمع البرافيني المدعم برغوة النحاس بمقدار عشرة أضعاف، بينما كان تأثير التهوية فعال لعدد من الساعات بعد غياب الشمس. اكبر معدل للتدفق الكتلي مع الجامع الشمسي ذي صندوق الخزن الحراري تم تسجيله بمقدار .36.65kg/hr عند معامل تدفق كتلي للمنظومة بمقدار 0.371 كذلك أظهرت النتائج بأفضلية الزاوية العاملة عند 60^o-45. بينما كان افضل تقارب في درجة حرارة الهواء الى درجه حرارة الجامع الشمسي والتي ظهرت عند المدخنة الشمسية ذات الممرين. أظهر تحليل النتائج العملية الحسابية ان اعلى كفاءة خزن حراري كانت بمقدار 47% عند معامل الاشعاع الشمسي 780 W/m^2 عند 12:00 pm, بينما مجموع الطاقة الحرارية خلال فترة الشحن كانت 18460 kJ , كما أشاره النتائج الى ان المدخنة ذات الممر الهوائي المزدوج وعند زاوية ميل 60^o أظهرت اعلى كفاءة حرارية 73% اما مدخنة الهواء الشمسية بممرين ومجمع خازن للحرارة فقد أظهرت اعلى كفاءة حرارية بمقدار70%.

الكلمات الرئيسية: مدخنة شمسية، كفاءة، الشمع البرافيني، رغوة النحاس. مواد ثنائية الطور

1. INTRODUCTION

There are many studies carried out to decrease percentage of the carbon release by consumption from traditional energy, and those have been conducted by employing the renewable energy. Solar irradiance is one of the most important energy sources, especially in the day time. But, the decrease in the solar irradiance near the sun-set, or absence of the energy after sun-set, leads to searching for method to store the thermal energy through day time and release it after sun-set or in the night time. Most of studies (experimental or numerical or both) employing solar chimney for heating or cooling and ventilation without using heat storage, calculated the instantaneous efficiency only; **(Ong & Chow, 2003; Ryan, et al., 2005; Burek & b., 2007; Paraphanpong, et al., 2010; Visagavel & P., 2010; Languri & Ganji, 2011; Robinson, et al., 2013; Amori & Hmood, 2013; Salah & Adel, 2013; Manaa, et al., 2013; Milad, 2015; Valmeti & Babu, 2017)** by dividing heat gain to the solar irradiance that lays on the SC collector. While, other studies depend on exhibiting the relation between the air temperature and time to define the efficiency of thermal system. Other studies used thermal energy storage material **(Fath, 1995; Sharma, et al., 2005; Sharma, et al., 2006; Sharma, et al., 2007; Alkilani , et al., 2009; Ojike, 2011; Amori & Mohammed, 2012; Jun, et al., 2017)** for different effects, many of these studies estimated the effect of heat storage with time, or estimated the instantaneous efficiency for solar chimney and neglected the heat storage, and at the same time they avoided estimating the real thermal efficiency in the periods of charging and discharging heat in the thermal energy storage material. So in this study, the thermal efficiency of solar collector is analyzing through the periodic time for charging and discharging depending on experimental with computational results.

2. EXPERIMENTAL SET-UP

2.1. Rig set-up

Three different types of solar chimney were tested with ventilation mode. SCs types are single pass and double passes flat plate collector, and double pass TESB collector. Those different SCs were installed to the south wall of insulated test room. To enhance heat transfer inside the thermal storage material for tilted SC, so semi refined paraffin wax with melting temperature range (48~54℃) was supported by copper foam matrix with 95% porosity and porous per inch (ppi) equal to 30. A vertical preheat SC with full refined paraffin wax and CFM were installed before the tilted SC with($T_m = 58{\sim}62$℃). The vertical SC was supported by array of evacuated tubular collector with a thermosyphon to collect the solar irradiance and charge TES material, also a direct irradiance was collected by the face surface of vertical TESBC, as shown in **Figs.1, 2,** and **3**.

2.2. Measurement and instruments tools

Data acquisition system with more than 100 thermocouple probes was used to read the temperature in each surface of collector, inside thermal storage material, temperature of air through the SC, transparent acrylic cover and else. Also, a high accuracy digital anemometer was employed to measure the air velocity in different locations and different levels through solar chimney gap. Modern solar intensity readers with weather station were installed to the test room.

2.3. Effective dimensions of the system

The most important effective dimension was the aspect ratio (ar) of SC (ratio of solar chimney length to its gap). The ar design value was depending on the optimum value at 12/1. So, the final design value for ar equals 25/1 for single pass SC and 50/1 for each pass of double passes SC. Depending on the designed value of ar, **Fig. 2**, so other dimensions of SC will be limited. For tilted SC, the length was 1.5 m and width 0.75 m, chimney gap equals 6 cm in single pass and 3 cm for each pass in the double passes SC. The Thermal Energy Storage Box (TESB) (PCM-CFM) in vertical SC has dimensions 1*0.75*0.025 m, while the tilted TESB has dimensions 1.5*0.75*0.025 m, and the weight factor (wax / combined) represents 59.48%.

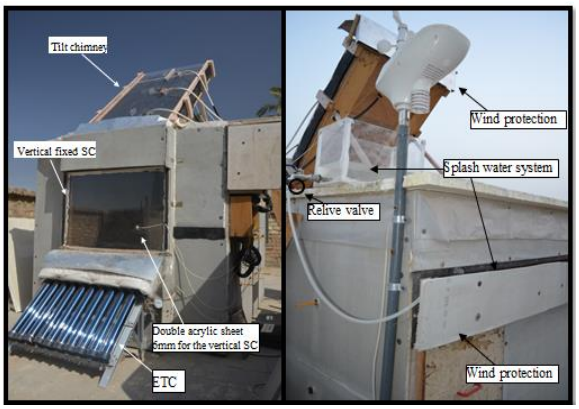

Figure 1. Test room with a vertical and tilted SC that used (PCM-CFM) as thermal energy storage material.

The insulated test room has dimensions (2*1.5*1.5) m, supported by SC's in south wall. Length of the test room is bigger than width and height, to clarify the behavior of temperature distribution inside room. Structure of test room consists of a wooden frame, insulated by cork and glass wool.

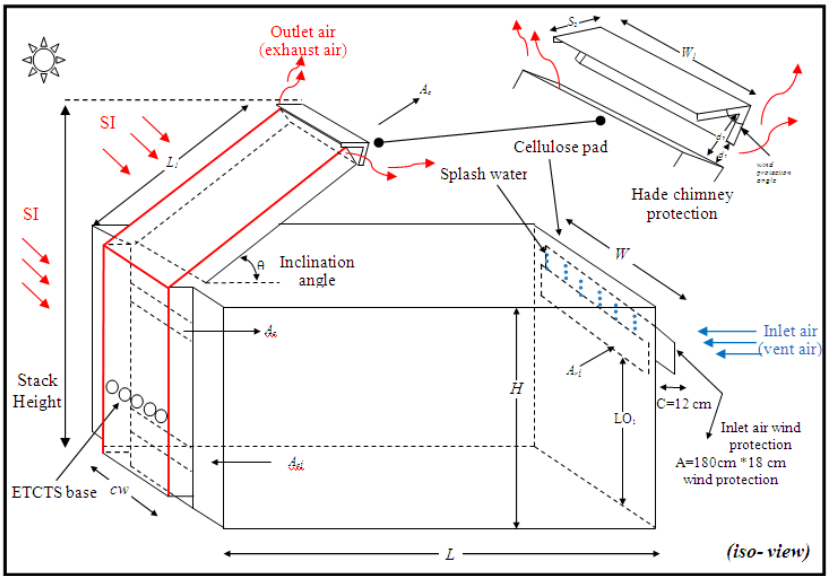

Symbol	Describe
W	Width of the test room 48 (cm)
H	High of the test room 147 (cm)
L	Length of the test room 200 (cm)
CW	Chimney Width 75 (cm)
L_1	Inclined chimney length 150 (cm)
W_1	Head chimney protection width 91 (cm)
$\theta 1$	Head chimney protection angle 90 (degree)
Lo1	Height from vent opening to base 115(cm)
θ	Inclination angle of tilted chimney 30^o, 45^o, 60^o
Aci	Opening area inlet to the chimney (75 *11) cm
SI	Solar Intensity direction
S_1	Head chimney protection side length 20 (cm)

Figure 2. Schematic diagram of insulated test room with ventilation and evaporative cooling modes.

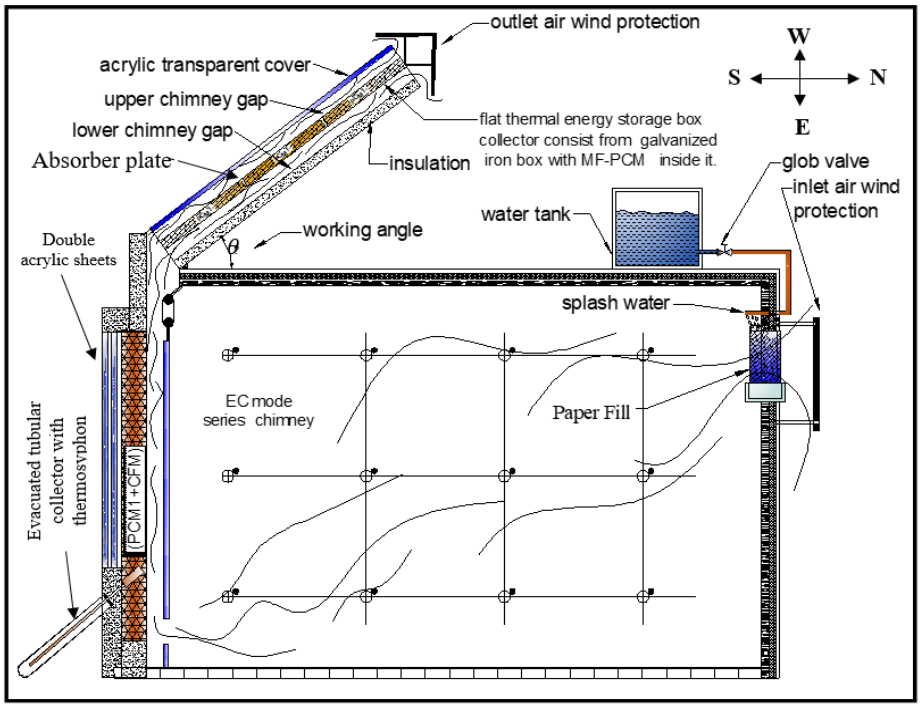

Figure 3. Schematic diagram describing the test room in ventilation and evaporative Cooling mode and depicting the vertical and tilted SC with thermal energy storage box.

3. THE SOLAR CHIMNEY (SC)

The system of ventilation that used SC consists of a vertical SC and tilted SC, both of them are connected together in series. Vertical solar chimney (preheat SC) depended on the evacuated tubular collector with a thermosyphon beside the transparence covered collector that was employed to collect the heat from the solar irradiance, **Fig. 3**. In vertical collector, the heat storage inside the combined of PCM-CFM. In tilted solar chimney, three different types of collector were used as mentioned previously. Single pass flat plate collector is show in **Fig. 5**, double passes flat

plate collector in **Fig. 6**, and double passes flat thermal energy storage box collector in **Fig. 7**. The third collector depended on the PCM-CFM to store the heat and release it after sun-set.

3.1Thermal energy storage material

To store the heat energy and release it in active time, the heat must be transferred in a limited duration time, and that means limit the value of thermal conductivity of the storage material. So, a CFM with 95% porosity and 30 porous per inch (ppi) was employed to support the main storage material (paraffin wax), **Fig. 4**.

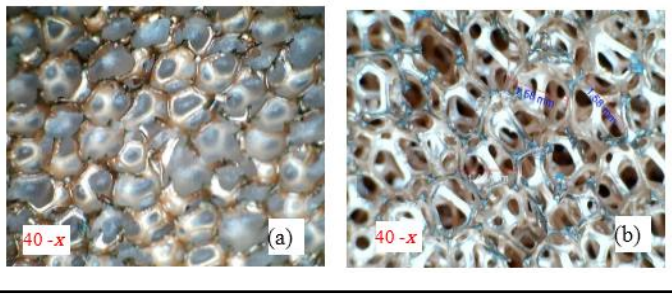

Figure 4. Copper foam matrix, a-with PW, b-without PW.

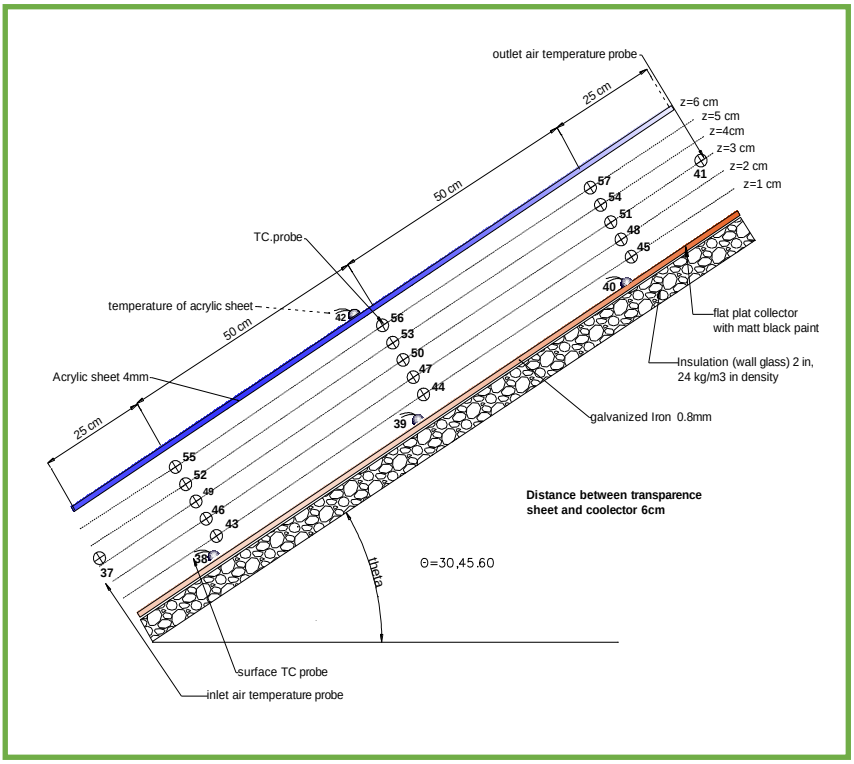

Figure 5. Single pass tilted solar chimney with flat plate collector.

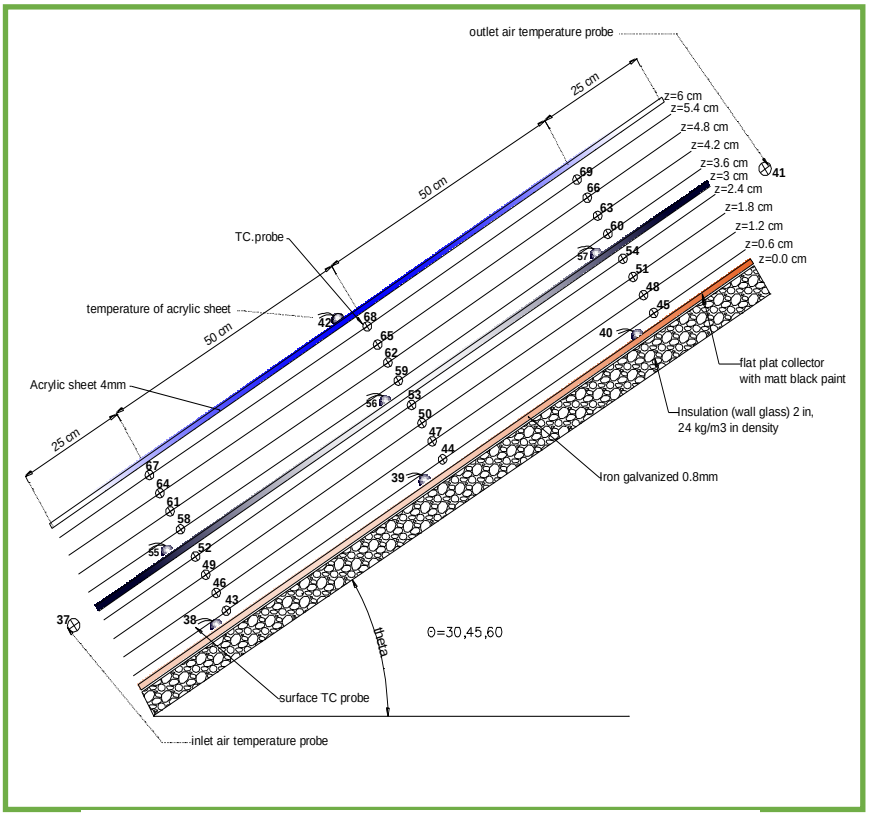

Figure 6. Double passes tilted solar chimney with flat plate collector.

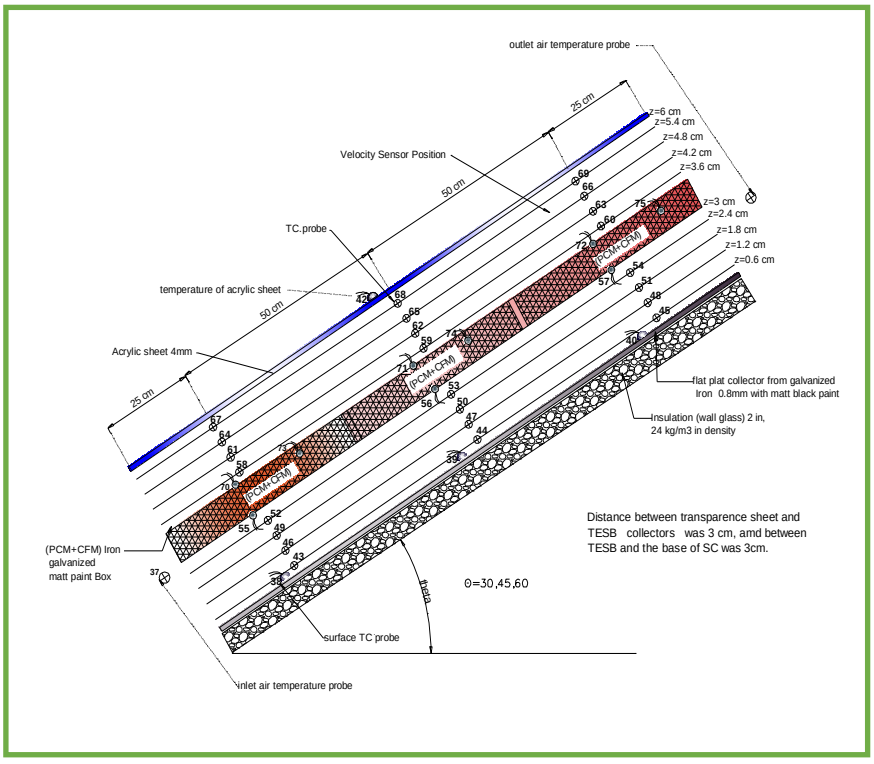

Figure 7. Double passes tilted solar chimney with thermal energy storage collector.

3.2 Effective thermal conductivity

The effective thermal conductivity for the combined PCM-CFM is defined by the Eq. (2), below **(Boomsma & Poulikakos, 2001, Yuan, 2012 and Tian & Zhao, 2013)**, where the averaging of the thermal conductivity of each section on the basis of the conductivities is down in the following manner:

$$k_n = \frac{V_{n,s}k_s + (V_n - V_{n,s})K_f}{V_n} \quad (1)$$

The effective thermal conductivity k_{eff} is a result of these four layers being placed in parallel, this thermal conductivity is calculated for each section (n: A, B, C, D) or (n:1,2,3,4) for the tetrakaidecahedron **(**the structure of a tetrakaidecahedron, which is a fourteen-face polyhedron comprising six squares and eight hexagons**) Fig. 8**. By using such a polyhedron approximation, **(Boomsma & Poulikakos, 2001)** obtained a good agreement between model predictions and experimental data on metal foams with porosities from 88% to 98%. The thermal conductivity through the representative section is calculated based on heat conduction through a series of four levels using Fourier's law of heat conduction to give the relation.

$$k_{eff} = \frac{L_A + L_B + L_C + L_D}{\left(\frac{L_A}{k_A}\right) + \left(\frac{L_B}{k_B}\right) + \left(\frac{L_C}{k_C}\right) + \left(\frac{L_D}{k_D}\right)} \quad (2)$$

Substituting the equation for the section lengths (L_n), the thermal conductivities for each (k_n), and the positive solution for d from Eq. (3)

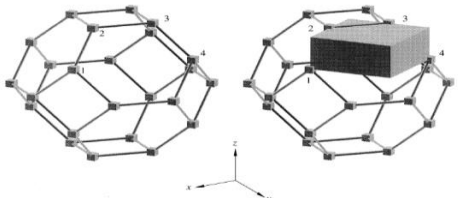

Figure 8. The tetrakaidecahedron modeled with cylindrical ligaments and cubic nodes.

$$d = \sqrt{\frac{\sqrt{2}\left(2 - \left(\frac{5}{8}\right)e^3\sqrt{2} - 2\varepsilon\right)}{\pi(3 - 4e\sqrt{2} - e)}} \quad (3)$$

yields a lengthy equation for the effective thermal conductivity as a function of the porosity, e, and d (which is a solved function of ε and e from Eq.(4))

$$\varepsilon = 1 - \frac{\sqrt{2}}{2}\left(de^2 + \frac{1}{2}\pi d^2(1-e) + \left(\frac{1}{2}e - d\right)e^2 + \pi d^2\left(1 - 2e\sqrt{2}\right) + \frac{1}{4}e^3\right) \quad (4)$$

Introducing the simplifying notation gives,

$$R_A = \frac{4d}{\left(2e^2 + \pi d(1-e)\right)k_s + (4 - 2e^2 - \pi d(1-e))k_f} \quad (5), \quad R_B = \frac{(e-2d)^2}{(e-2d)e^2k_s + (2e - 4d - (e-2d-(e-2d)e^2)k_f} \quad (6)$$

$$R_C = \frac{(\sqrt{2}-2e)^2}{2\pi d^2\left(1-2e\sqrt{2}\right)k_s + 2(\sqrt{2} - 2e - \pi d^2(1-2e\sqrt{2}))k_f} \quad (7), \quad R_D = \frac{2e}{e^2k_s + (4-e^2)k_f} \quad (8)$$

Finally, this yields the final result of the effective thermal conductivity to be:

$$\bar{k}_{PCM-MF} = \frac{\sqrt{2}}{2(R_A + R_B + R_C + R_D)} \quad (9)$$

Where, $e = 0.339$, k_s: Thermal conductivity of the material used to manufacture the metal foam. k_f: Thermal conductivity of the material saturated in the metal foam. R_A, R_B, R_C and R_D: Thermal resistance of four different layers inside a tetrakaidecahedron cell. The effective thermal conductivity $\bar{k}_{PCM-MF}$ is a result of these four thermal layers placed in parallel.

Other properties of the combined, like density and specific heat, can be estimated from the general equations as shown below **(Vadwala, 2011)**:

$$\varphi_{eff} = (1 - \varepsilon)\varphi_x + \varepsilon\,\varphi_y \quad (10)$$

$$\varphi_{eff-x} = (1-\varepsilon)\varphi_{Px} \quad (11)$$

$$\varphi_{eff-y} = \varepsilon\varphi_{Px} \quad (12)$$

$\varphi =$ Physical properites, $\varepsilon =$ CFM porosity or porosity of material, and $x, y =$ Material type

3.3 Equivalent heat capacity

To calculate the effective specific heat for paraffin wax in the mushy zone **Fig. 9**, as shown below;

$$C_{P-eff} = \frac{h_{s-l,wax}}{\Delta T_{mushy}} + C_{P,av} \quad (13)$$

$$C_{P,av} = \frac{1}{2}\left(C_{P,S} + C_{P,l}\right) \quad (14)$$

So, by defining the Equivalent Heat Capacity Method,

$$C_P = \begin{cases} C_{P,S} & T < T_m - \Delta T \\ C_{P,SL} & T_m - \Delta T < T < T_m + \Delta T \\ C_{P,L} & T > T_m + \Delta T \end{cases} \quad (15)$$

If the latent heat of fusion is known, and specific heat for solid and liquid with ΔT, the specific heat of mushy zone Eq. (13) can be defined as shown in **Fig. 9**. To estimate the heat, transfer by conduction or heat storage in materials, so it must be defined the properties of materials that consist of the galvanized steel, acrylic, copper foam matrix and the properties of paraffin wax at solid and liquid state. To simplify the computational model, the physical fact that the phase change taken place in a temperature interval $(T_m \pm \Delta T_m)$ can be employed. So, the heat balance equations that describe the heat storage and heat transfer during phase change can be divided as regions state: solid, liquid and mushy zone.

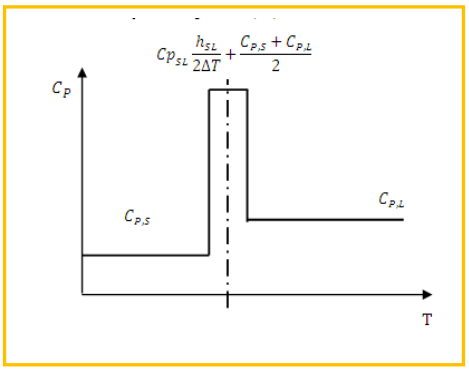

Figure 9. Specific heat value for paraffin wax in solid liquid and mushy zone.

For solid phase or state, $\rho_s, C_{P,s}, k_s$ $\quad T < T_m - \frac{\Delta T_m}{2}$ (16)

For liquid phase, $\rho_l, C_{P,l}, k_l$ $\quad T > T_m - \frac{\Delta T_m}{2}$ (17)

For mushy zone, $\rho_m, C_{P,m}, k_m$ $\quad T_m - \frac{\Delta T_m}{2} \leq T \leq T_m + \frac{\Delta T_m}{2}$ (18)

Many methods are defined to describe the phase change. The effective heat capacity method is the one of the simplest and effective methods to estimate the heat transfer or heat storage in the different three regions. With a narrow temperature difference in mushy zone, this method depicts the most precise method.

3.4 Effective heat capacity method

In this method, the latent heat effect is expressed as a finite temperature dependent on the specific heat that occurs over the temperature range. In this method, it is possible to describe the non-isothermal phase change. So, the effective (equivalent) heat capacity during the phase change can be presented as shown in the equation **(Ahmed, 2010)**:

$$C_{P,eff} = \frac{h_{sl}}{\Delta T_m} + C_{P,av} \quad (19)$$

ΔT_m Is the mushy zone difference temperature, h_{sl} means the value of latent of fusion to define the average heat capacity $C_{P,av}$,

$$C_{P,av} = \frac{1}{2}\left(C_{P,s} + C_{P,l}\right) \quad (20)$$

For incompressible fluid and for solid, it is possible to change C_P instead of C_V as shown above and with acceptable error.

To define the new set of properties of PCM by melting process for a small unit volume, **Fig. 10** shows the time-dependent temperature of unit volume of phase change material during T_1 and T_2. The density of PCM can be estimated by arithmetic average:

$$\rho_m = \frac{1}{2}(\rho_s + \rho_l) \quad at \quad T_m - \frac{\Delta T_m}{2} \le T \le T_m + \frac{\Delta T_m}{2} \quad (21)$$

For the compound of copper foam matrix and phase change material, the density can be defined as **(Vadwala, 2011)**:

$$\rho_{PCM-CFM} = (1-\varepsilon)\rho_{CFM} + \varepsilon\rho_{PCM} \quad (22)$$

For pure PCM, it is defined as:

$$k_m = \frac{1}{2}(k_s + k_l) \quad at \quad T_m - \frac{\Delta T_m}{2} \le T \le T_m + \frac{\Delta T_m}{2} \quad (23)$$

While, the thermal conductivity is defined in mushy zone as shown in below for the compound of the PCM-CFM, as effective value. The specific heat can be defined for the PCM-CFM as:

$$C_{P,PCM_m-CFM} = (1-\varepsilon)C_{P,CFM} + \varepsilon C_{P,PCM_m} \quad \text{at} \quad T_m - \frac{\Delta T_m}{2} \le T \le T_m + \frac{\Delta T_m}{2} \quad (24)$$

$$\varepsilon = \frac{\text{bulk volume} - \text{metal volume}}{\text{bulk volume}} 100\% = \text{porosity}$$

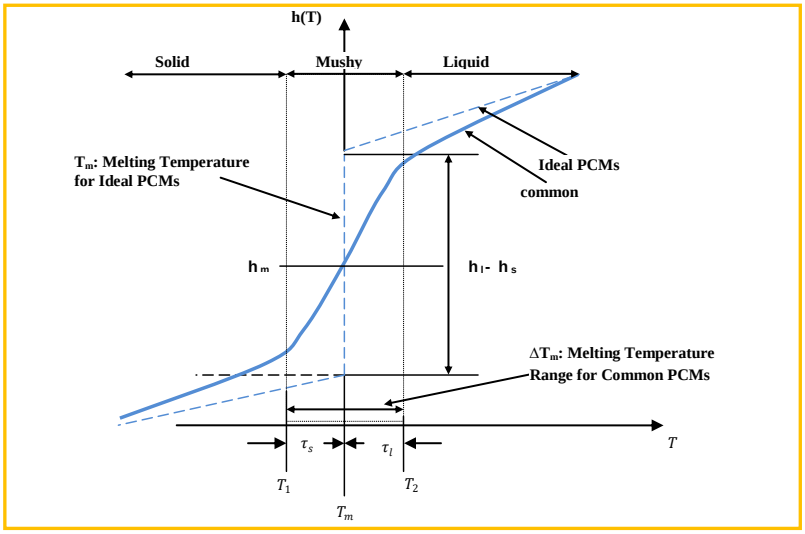

Figure 10. Mushy zone for phase change material.

3.5 Energy storage and release

By defining the new properties of the heat storage material, the storage or release energy in a control volume of the compound q^V may be expressed as:

$$q^V = \int_{T_i}^{T_1} \rho_s\, C_{P,s}\, dT + \int_{T_1}^{T_2} \rho_m\, C_{P,m}\, dT + \int_{T_2}^{T_l} \rho_l\, C_{P,l}\, dT \quad (25)$$

$$q^V = \varepsilon \int_{T_i}^{T_1} \rho_{s-PCM}\, C_{P,s-PCM}.dT + (1-\varepsilon) \int_{T_i}^{T_1} \rho_{CFM}\, C_{P-CFM}.dT + \varepsilon \int_{T_1}^{T_2} \rho_m\, C_{P-m}.dT$$

$$+(1-\varepsilon) \int_{T_1}^{T_2} \rho_{CFM}\, C_{P-CFM}.dT + \varepsilon \int_{T_2}^{T_l} \rho_{l-PCM}\, C_{P,l-PCM}.dT$$

$$+(1-\varepsilon) \int_{T_2}^{T_l} \rho_{CFM}\, C_{P-CFM}.dT \quad (26)$$

$$q^V = \{\varepsilon(\rho_{s-PCM}C_{P,s-PCM}) + (1-\varepsilon)(\rho_{CFM}C_{P-CFM})\}(T_1 - T_i) + \{\varepsilon(\rho_m C_{P-m})$$

$$+(1-\varepsilon)\big(\rho_{CFM}C_{P-CFM}\big)\}(T_2 - T_1) + \{\varepsilon(\rho_{l-PCM}C_{P,l-PCM}\big) + (1-\varepsilon)$$

$$(\rho_{CFM}C_{P-CFM})\}(T_l - T_2) \quad (27)$$

$$T_1 = T_m - \tfrac{\Delta T_m}{2}\,, \qquad T_2 = T_m + \tfrac{\Delta T_m}{2}, \qquad T_1 - T_i = T_m - \tfrac{\Delta T_m}{2} - T_i \quad (28)$$

$$T_2 - T_1 = T_m + \tfrac{\Delta T_m}{2} - T_m + \tfrac{\Delta T_m}{2} = \Delta T_m\,, \qquad T_l - T_2 = T_l - T_m - \tfrac{\Delta T_m}{2} \quad (29)$$

$$q^V = \{\varepsilon(\rho_{s-PCM}C_{P,s-PCM})$$

$$+(1-\varepsilon)\left(\rho_{CFM}C_{P-CFM})\right\}\left(T_m - \frac{\Delta T_m}{2} - T_i\right) + \left\{\varepsilon\left(\frac{\rho_m h_{ls}}{\Delta T_m}\right) + \frac{\rho_{s-PCM}C_{Ps-PCM} + \rho_{l-PCM}C_{Pl-PCM}}{2}\right.$$

$$+ (1-\varepsilon)\big(\rho_{CFM}C_{P-CFM}\big)\}(\Delta T_m) + \{\varepsilon(\rho_{l-PCM}C_{P,l-PCM}\big) +$$

$$(1-\varepsilon)(\rho_{CFM}C_{P-CFM})\}\left(T_l - T_{m-}\tfrac{\Delta T_m}{2}\right) \quad (30)$$

By assuming no big change in the properties at the same material constant values;

$\rho_{CFM},\ C_{P-CFM},\ \rho_{l-PCM},\ \rho_{S-PCM},\ C_{P,s-PCM},\ C_{P,l-PCM},\ \varepsilon, T_m,\ \Delta T_m$

can be entered in the subroutine- program as general constants.

Let;
$$\left.\begin{array}{c} x_1 = \varepsilon\big(\rho_{s-PCM}C_{P,s-PCM}\big),\ x_2 = (1-\varepsilon)(\rho_{CFM}C_{P-CFM}), x_3 = \varepsilon\rho_m h_{ls} \\ x_4 = \frac{\rho_{s-PCM}C_{Ps-PCM} + \rho_{l-PCM}C_{Pl-PCM}}{2}, x_5 = \varepsilon(\rho_{l-PCM}C_{P,l-PCM}) \end{array}\right\} \quad (31)$$

Eq. (30) can be re-written as:

$$q^V = \left\{(x_1 + x_2)\left(T_m - \frac{\Delta T_m}{2} - T_i\right)\right\} + \left\{\left(\frac{x_3}{\Delta T_m} + x_4 + x_2\right)\Delta T_m\right\}$$

$$+\left\{(x_5 + x_2)\left(T_l - T_m - \tfrac{\Delta T_m}{2}\right)\right\} \quad (32)$$

3.6 Simultaneous efficiency of heat storage

The simultaneous efficiency at the duration time of heat charge, can be compute from the rate of heat storage in TESB during its exposure to the solar radiation which can be calculated from the eqn. below;

$$q = m\Delta h/t=(m_{wax}\Delta h_{wax} + m_{copper}C_{copper}\Delta T_{copper})/t \quad (33)$$

Where, m= mass for wax and copper foam matrix.

t: duration time to charge TESB by heat (q).

So, the heat storage in the duration time t can be found from Eq. (34)

$$Q = q.t \quad (34)$$

The heat storage during the duration charge for N time can be computed by algebraic summation of Eq. (33) to get

$$Q_{total} = \sum_{n=1}^{N}\{m_{wax}\Delta h_{wax} + m_{copper}C_{copper}\Delta T_{copper}\} \quad (35)$$

Thus, the ratio of the heat storage to the heat absorbed by TESB is

$$\eta = \frac{Q_{storage}}{Q_{absorbed}} = \frac{\{m_{wax}\Delta h_{wax}+m_{copper}C_{copper}\Delta T_{copper}\}}{I_{beam}.A_a.\alpha_a.t} \quad (36)$$

4. TILTED SOLAR CHIMNEY EFFICIENCY

The tilted SC efficiency in ventilation mode with different collector configuration and in different inclination angles, is evaluated by employing the data result as shown below:

4.1 The efficiency for single pass SC collector

$$\eta_{SC} = \frac{Q_{load}}{Q_{solar}} = \frac{m_{air}\dot{C}_P\Delta T}{I_r\, A\, (1-\tau)} \quad (37)$$

τ: transmisivity of acrylic

I_r: solar irradiance

A: area of solar collector

With assumption of no heat losses (small value) with good heat insulation.

4.2 The efficiency for double passes SC collector

Same as the calculation in the previous collector.

4.3 The efficiency for double passes TESB SC collector

There are three different evaluation values depending on change of solar irradiance with time and heat storage or release from the combined thermal storage material. The concluded diagram from this study in **Fig. 11** depicts the three different evaluation zones.

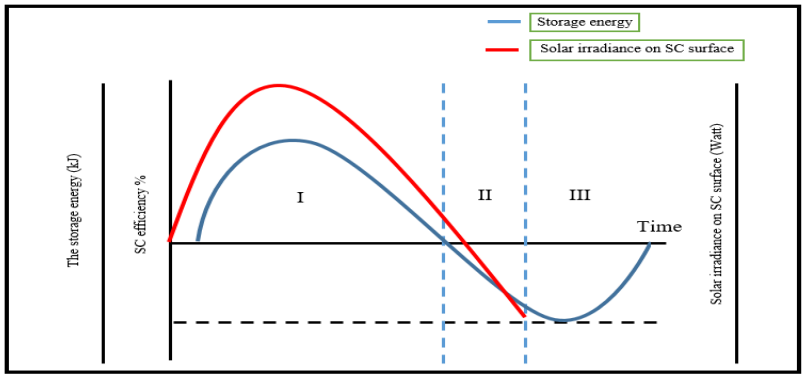

Figure 11. Diagram to defined solar chimney efficiency through day with heat storage or release.

$$\eta_{SC-I} = \frac{Q_{load}}{Q_{solar} - Q_{storage}} \quad (38) \qquad \eta_{SC-II} = \frac{Q_{load}}{Q_{solar} + Q_{storage}} \quad (39) \qquad \eta_{SC-III} = \frac{Q_{load}}{Q_{storage}} \quad (40)$$

Heat storage can be evaluated from the graph of energy storage efficiency.

5. EXPERIMENTAL TEST PROCEDURE

The experimental work was achieved in June, 2015, where data are logging for the dependent variables along 12 hours. All measurements and instruments tools were used as mentioned previously to measure and record the dependent variables, for each 2 hours as test interval, while the average value for general variables were measured and recorded by weather station data logger along 24 hours, with 20 minutes as test interval. Temperature was Measuring in chimney gap, test room space, TESB and outdoor respectively.

6. THEORETICAL CONSIDERATION

In this study, it is assumed that there are no heat losses directly from test room or from the insulated part of the solar chimney to the surround. So, according to the heat balance, the heat absorbed by collector must be equal to heat released to the working air that passes through the chimney gap for the flat plate collector in single and double passes. While in the TESB collector, the heat balance means the summation of heat released to the working fluid plus heat that stored or rejected from the compound thermal storage material.

7. RESULTS AND DISCUSSION

Fig. 12 reveals the heat storage efficiency with maximum value at 12:00 pm, because the higher difference in temperature between inside TESB and its up-surface collector (0.75*1.5) m^2 accrues at that time. Heat storage efficiency equals the summation of change of energy storage through time to the summation of solar energy through same time. To define the efficiency of approaching the air temperature can be compared with the collector surface temperature, as shown in **Figs.13, 14** and **15**. The result indicated that the best angle in single pass is 45~60^o, and the 60^o angle in the

double passes flat plate collector, while the two working angles 45^o and 60^o can be applied with good results to TESB collector. In **Figs. 16, 17** and **18**, a comparison for collector's temperature between different SC types and at the same working angle is presented. The working angle at 30^o showed that the increasing in collector temperature for single phase collector is more than other types (with low approaching for air to collector temperature), and the double passes flat plate collector is the lowest in temperature (with highest value in approaching). That means the single pass had a bad attachment between air and collector surface, while the double passes flat plate collector had a good attachment between air and surface collector (good heat transfer). Also, the highest value of aspect ratio (ar) gives a guarantee to prevent back air flow (movement) in chimney gap and also induced air flow over surface collector with good contact (good heat transfer). TESB collector, storage heat energy that releases after sunset for long time. So, it still has higher temperature after sunset and provides the system by the heat needed. **Figs. 19, 20** and **21** present the thermal efficiency for the three types tilted solar collector with different angles. The results appeared clearly the positive effect for the angle, that means of at vertical SC, the difference pressure increases and leads to increasing in the air flow. Double passes SC at 60^o angle presents the highest efficiency with value approaching to 73%. TESB collector in **Figure 21** depicts the highest efficiency value 70% at 12:00 pm. One of more important notes, the double passes SC with TESB collector effect remains after sunset for a long time as shown in **Figs. 22, 23** and **24**, while the highest efficiency of storage energy was recorded at 60^o angle. Also, the increase of efficiency after sunset occurs, because the sharp decrease of outside temperature comparing with the hot collector leads to increasing the solar chimney efficiency.

8. CONCLUSION

Heat storage in the phase change material like wax is not efficient, because there is a bad thermal conductivity and that means bad heat transfer. To enhance the thermal conductivity, it is effective to employ CFM with high porosity to enhance the heat transfer. Heat storage in the combined material still releases heat energy after absence the heat source, and that refers to success for employing the paraffin wax with CFM as a TESM. To estimate the SC efficiency, a heat balanced equation between the solar irradiance and the heat that charge and release from the combined material PCM-CFM must be made during the experiment time (before sun rise, during day time and arriving to the night time (after sun set)).

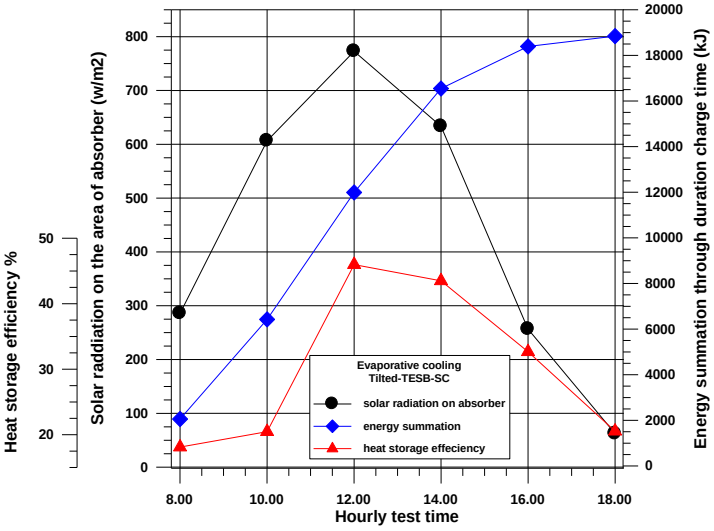

Figure 11. Solar radiation, energy summation and heat storage efficiency.

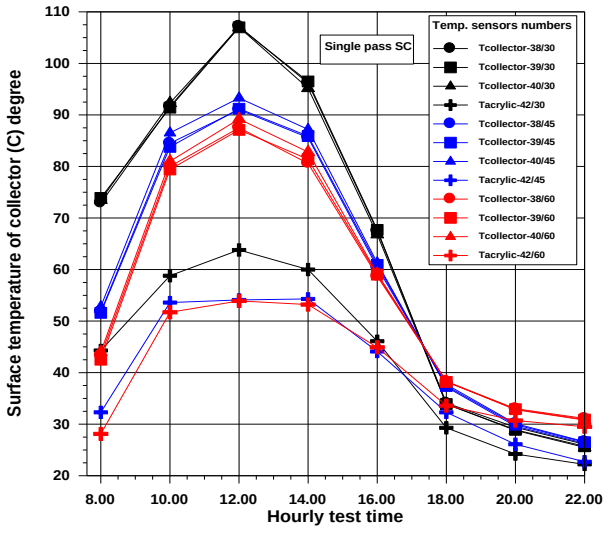

Figure 12. Solar radiation, energy summation and heat storage efficiency.

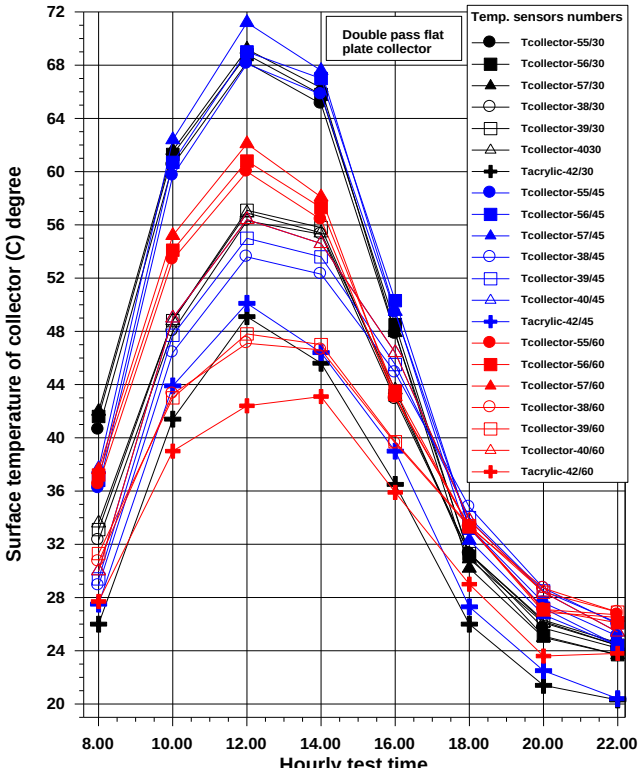

Figure 13. Comparison between the SCs temper for single pass, and in different in tilted angl

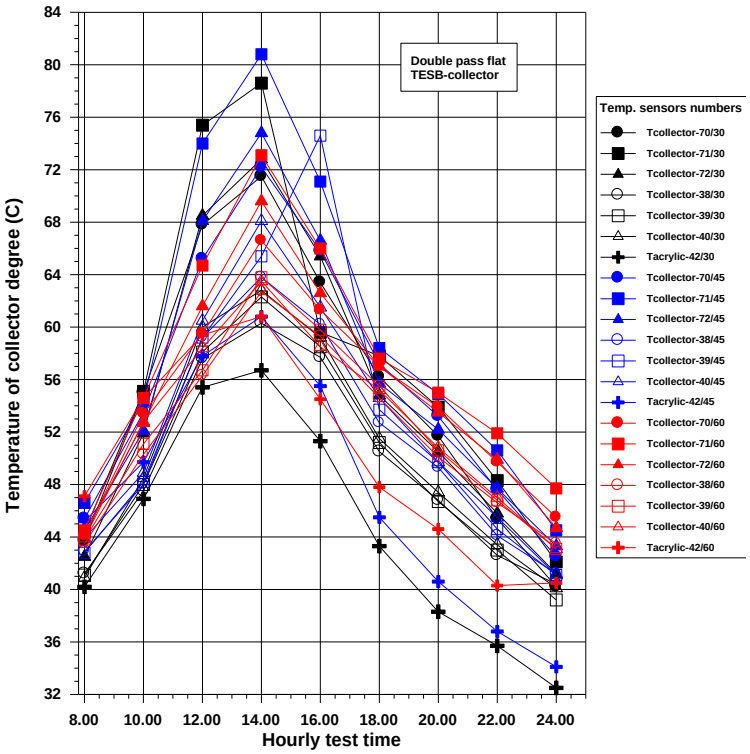

Figure 14. Comparison between the SCs temperatures for double pass flat plate collector and in different in tilted angle.

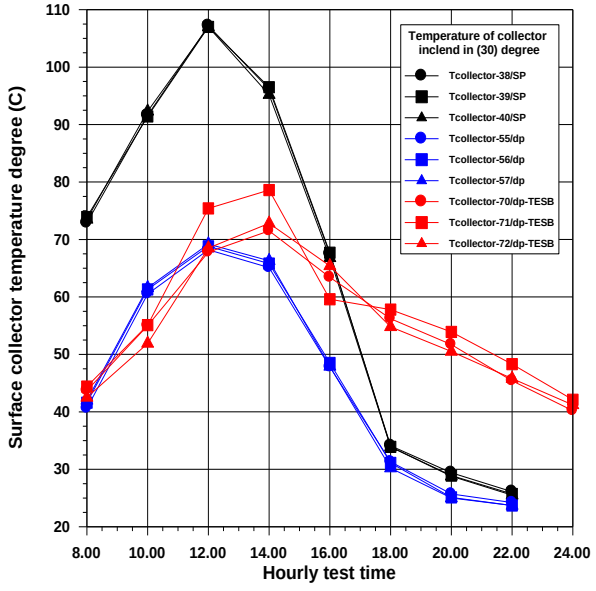

Figure 15. Comparison between the SCs temperatures for double pass TESB collector and in different in tilted angle**.**

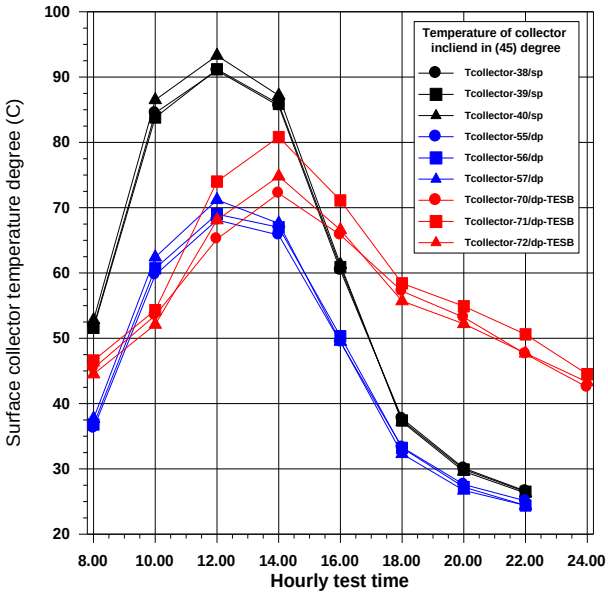

Figure 16. Comparison between the SCs Temperatures for three different types at 30^{o} of tilted angle.

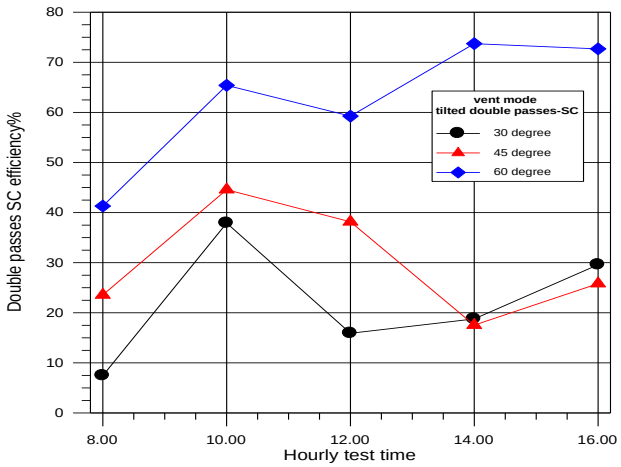

Figure 17. Comparison between the SCs Temperatures for three different types at 45° of tilted angle.

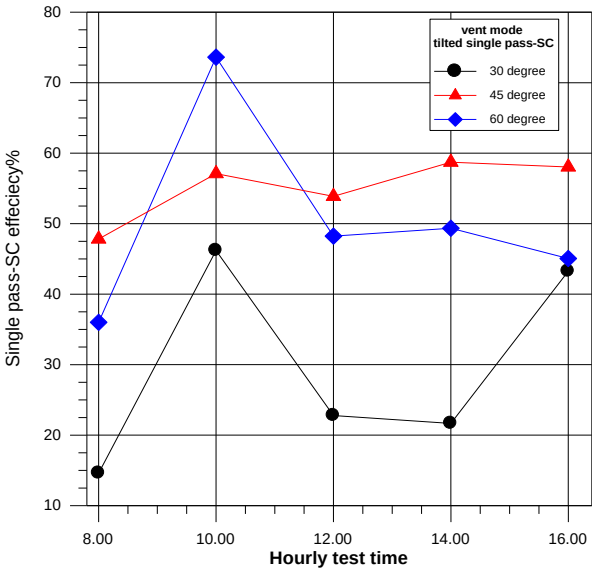

Figure 18. Comparison between the SCs temperatures for three different types at 60° of tilted angle.

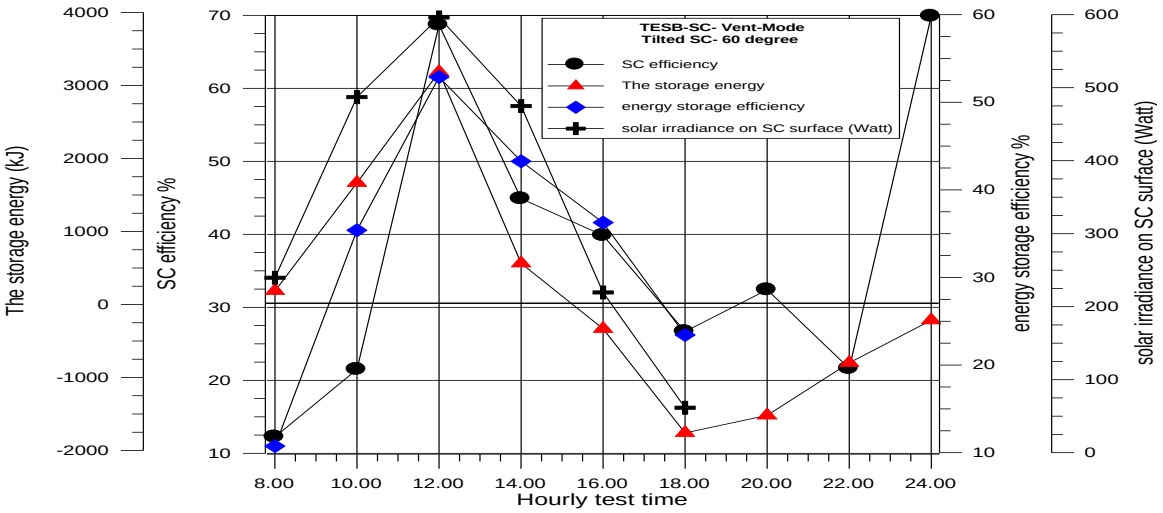

Figure 19. Single pass tilted flat plate solar chimney collector efficiency in ventilation mode.

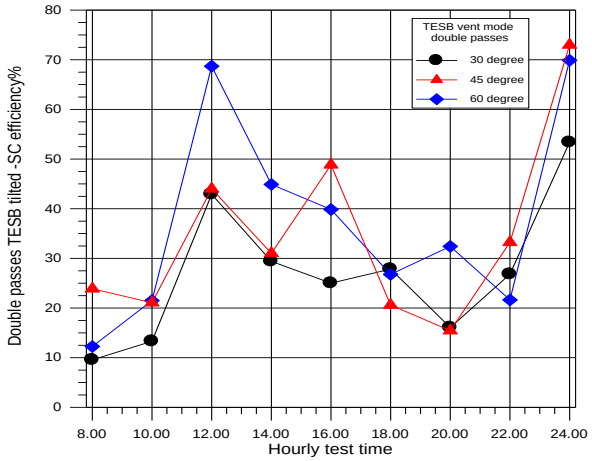

Figure 20. Double passes tilted flat plate solar chimney collector efficiency in ventilation mode.

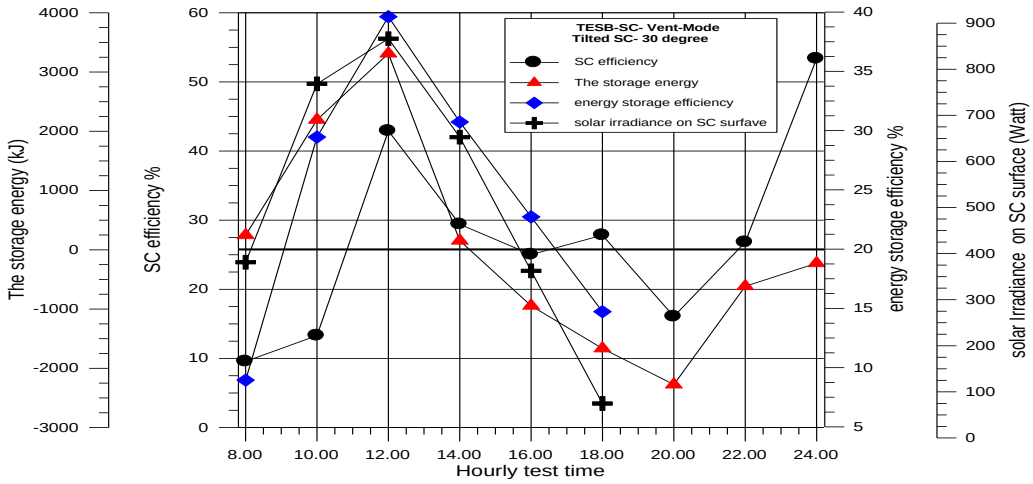

Figure 21. Double passes TESB tilted solar chimney collector efficiency in ventilation mode in different angle.

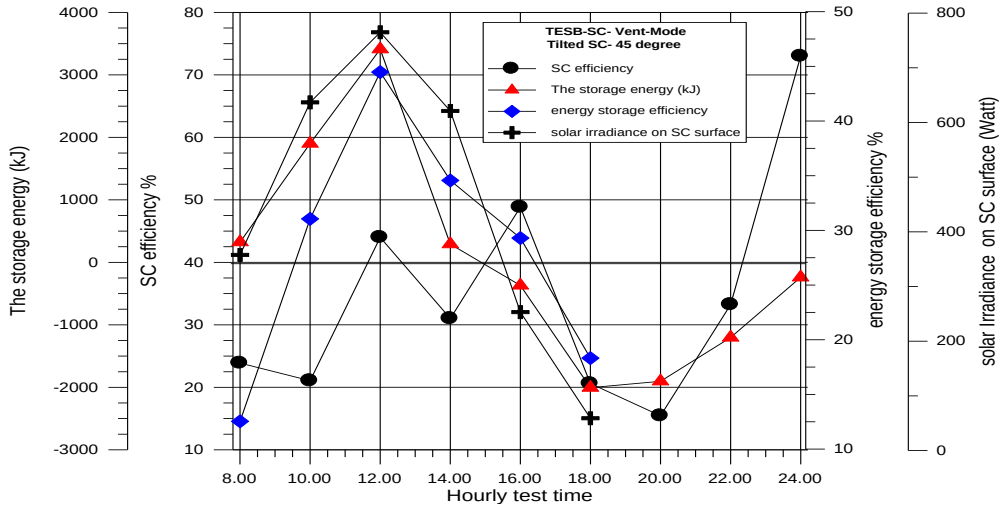

Figure 22. Double passes TESB tilted solar chimney collector efficiency in ventilation mode at 45-degree angle.

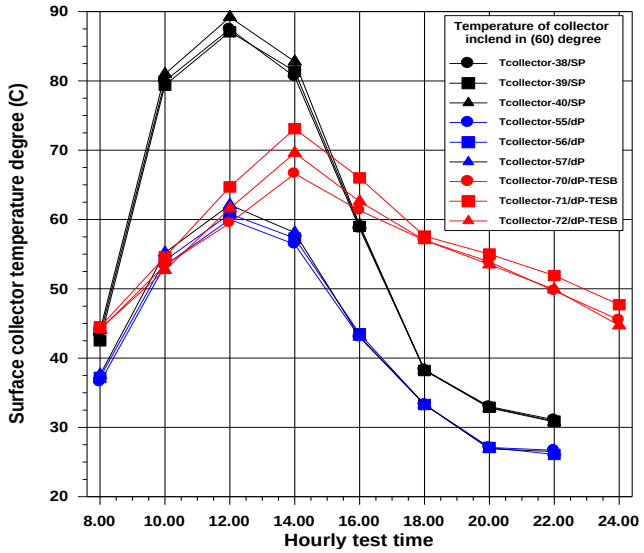

Figure 23. Double passes TESB tilted solar chimney collector efficiency in ventilation mode at 60-degree angle.

NOMENCLATURE

A	Area, m^2
ar	Dimensionless aspect ratio $(L/gap)_{SC}$
C_d	Discharge coefficient
C_p	Specific heat, kJ/kg. K
CFM	Copper Foam Matrix
FVM	Finite Volume Method
g	Gravitational acceleration, m/s^2
h	Enthalpy, height, kJ/kg, m
h	Heat transfer coefficient, W/m^2.K
h_{fu}, h_{fs}	Latent heat of fusion, kJ/kg
hr	Hour
I_{-beam}	Beam solar radiation, W/m^2
k	Thermal conductivity W/m. K
$k_{eff}(k_{PCM-CFM})$	Effective thermal conductivity of the PCM-embedded CFM , W/m. K
L	Length, m
m, $\dot{m}$	Mass, mass flow rate, kg, kg/s
n	A, B, C, D, (refer to the CFM sections in cell)
P	Point
PCM	Phase Change Material
ppi	Porous per inch
q''	Heat flux, W/m^2
Q'''	Internal heat generation rates, W/ m^3
SC	Solar Chimney
t	time, sec
T	Temperature, ℃, K
TESM	Thermal Energy Storage Material
TESMB	Thermal Energy Storage Material Box
V	Volume, m^3
$\dot{V}$	Volume flow rate, m^3/s

Greek letter

ρ	Density, kg/m^3
α	Diffusivity, m^2/s
θ	Solar chimney tilt angle, degree
η	Heat Storage Efficiency
ε	porosity

Subscripts

av	Average
eff	effect, effectiveness
l,2	Liquid, liquid state
m	Mushy, melting
n	Number of sections in material (CFM)
s,1	Solid, solid state
sl	Liquid –solid

REFERENCES

- Amori, K. E. & Hmood, K. N., 2013. , Numerical Study of Solar Chimney with Absorber at Different Locations. *Journal of Engineering*, 19(4), pp. 485-499.
- Amori, K. E. & Mohammed, S. W., 2012. Experimental and numerical studies of solar chimney for natural ventilation in Iraq. *Energy and Buildings* , Volume 47, pp. 450-457.
- A. M., S. K. & A. M., 2009. Using a Paraffin Wax-Aluminum Compound as a Thermal Storage Material in Solar Air Heater. *ARPN Journal of Engineering and Applied Sciences,* 4(10), pp. 74-77.
- B. Belfuguais; , Lerbi S., 2011. Passive Ventilation System Analysis usung Solar Chimney in South of Algeria. *World Academy of Science, Engineering and Technology,* Volume 58, pp. 26-30.
- Burek, S. A. & b., A. H., 2007. Air flow and thermal efficiency characteristics in solar chimneys and Trombe Walls. *Energy and Buildings* , Volume 39, pp. 128-135.
- C.-D. H., H.-M. Y. & T.-C. C., 2011. Collector of Upward-Type Double-Pass Solar Air Heater with Fins Attached. *International Communications in Heat and Mass Transfer,* Volume 38, pp. 49-56.
- Fath, H. E., 1995. Transient Analysis of Thermosyphon Solar Air Heater with Built-In Latent Heat Thermal Energy Storage System. *Renewable Energy,* 6(2), pp. 119-124.
- H. K. et al., 2005. *Development of Solar Chimney with Built-In Latent Heat Storage Material for Natural Ventilation.* Hamamatsu, Japan, EXPO World Conference on Wind Energy, Renewable Energy, Fuel Cell & Exhibition .
- J. L., X. G., Q. L. & Y. L., 2017. Thermal Storage Capacity and Night Ventilation Performance of a Solar Chimney Combined with Different PCMs. *Hindawi International Journal of Photoenergy,* pp. 1-10.
- K. B. & D. P., 2001. On the Effective Thermal Conductivity of a Three-Dimensionally Structured Fluid-Saturated Metal Foam. *International Journal of Heat and Mass Transfer* , Volume 44, pp. 827-836.
- Languri, E. M. & Ganji, D. D., 2011. *Thermal Aspects of Solar Air Collector.* [Online].
- M. B., 2015. Numerical Investigation of Thermal Performance of Double Pass Solar Air Heaters. *IJBPAS,* 4(8)(Special Issue), pp. 186-204.
- Ong, K. S. & Chow, C. C., 2003. Performance of aSolar Chimney. *Solar Energy 74,* pp. 1-17.
- O. O., 2011. Characterization of a Flat Plate Double Glazed Solar Collector. *Continental J. Renewable Energy* , Volume 2(2), pp. 10-18.
- P. S., U. T. & W. S., 2010. Investigation of Buoyancy Air Flow inside Solar Chimney using CFD Technique. *Technique Proceedings of the International Conference on Energy and Sustainable Development,* Issue Issues and Strategies, pp. 1-7.

- Robinson, B. S. et al., 2013. Heating Season Performance of a Full-Scale Heat Pipe Assisted Solar Wall. *Solar Energy* , pp. 76-83.
- Ryan, D. A., S. B. & P. B., 2005. Experimental Investigation Into the Buoyancy Driver Convection in Passive Solar Heating Facades. *Rotterdam (Netherland) in-house puplishing,* pp. 683-693.
- Sharma, S. D. et al., 2007. Design, Development of a Solar Chimney with Built-In Latent Heat Storage Material for Natural Ventilation. *International J. of Energy,* 4(3), pp. 313-324.
- S. L. & A. E. H., 2013. Thermo-fluid aspect analysis of passive cooling system case using solar chimney in the south regions of Algeria. *Energy Procedia ,* Volume 36, pp. 628-637.
- S. M. et al., 2013. Simulation of a combination of a solar air collector and a stock for a solar drying in Algeria. *Energy Procedia ,* Volume 36, pp. 386-390.
- Taha, A. K., 2010. Simulation of Heat Storage and Heat Regeneration in Phase Change Material. *MSc Thesis, University of Baghdad.*
- Vadwala, P. H., 2011. *Thermal Energy Storage in Copper Foams filled with Paraffin Wax.* Msc. Thesis ed. University of Toronto: Mechanical & Industrial Engineering.
- V. K. & P. S., 2010. Experimental Investigation on Solar Air Heater Assisted Natural Ventilation in Single-Sided Ventilated Room. *Indian Journal of Science and Technology,* 3(7), pp. 802-806.
- V. S. & Babu, B. S., 2017. Computational Fluid Dynamics Analysis of A Building Ventilation Solar Chimney. *IJARIIE,* 2(2), pp. 106-109.
- Y. K. et al., 2006. Ventilation Performance of Solar Chimney with Built－in Latent Heat Storage. *Proceeding of international Conf. on Thermal Energy Storage.*
- Y. T., 2012. Heat Transfer Enhancement in Phase Change Materials (PCMs) by Metal Foams and Cascaded Thermal Energy Storage. *PhD, Thesis, University of Warwick.*
- Y. T. & Zhao, C. Y., 2013. Thermal and Exergetic Analysis of Metal Foam-enhanced Cascaded Thermal Energy Storage (MF-CTES). *International Journal of Heat and Mass Transfer* , Volume 58, pp. 86-96.